Electronic Supplementary Material to: What Drives the Decadal Variability of Global Tropical Storm Days from 1965 to 2019? *

Yifei DAI[1,2], Bin WANG[1,2,3], and Weiyi SUN[2,4]

[1]*Key Laboratory of Meteorological Disaster of Ministry of Education, and Earth System Modeling Center, Nanjing University of Information Science and Technology, Nanjing* 210044, *China*

[2]*International Pacific Research Center, University of Hawaii at Manoa, Honolulu, HI* 96822, *USA*

[3]*Department of Atmospheric Sciences, School of Ocean and Earth Science and Technology, University of Hawaii at Manoa, Honolulu, HI* 96822, *USA*

[4]*Key Laboratory for Virtual Geographic Environment. Ministry of Education; State Key Laboratory Cultivation Base of Geographical Environment Evolution of Jiangsu Province; Jiangsu Center for Collaborative Innovation in Geographical Information Resource Development and Application; School of Geography Science, Nanjing Normal University, Nanjing* 210023, *China*

ESM to: Dai, Y. F., B. Wang, and W. Y. Sun, 2022: What drives the decadal variability of global tropical storm days from 1965 to 2019? *Adv. Atmos. Sci.*, **39**(2), 344–353, https://doi.org/10.1007/s00376-021-0354-1.

Table S1. Correlation Coefficients among global integrated annually mean TSD, TSG, ACE, PDI, and LS. All the correlation coefficients are statistically significant at the 99% confidence level, except for the one between TSG and LS.

	TSD	TSG	ACE	PDI	LS
TSD	—	0.72	0.88	0.79	0.69
TSG	0.72	—	0.57	0.49	0.09
ACE	0.88	0.57	—	0.98	0.65
PDI	0.79	0.49	0.98	—	0.60
LS	0.69	0.09	0.65	0.60	—

*The online version of this article can be found at https://doi.org/10.1007/s00376-021-0354-1.

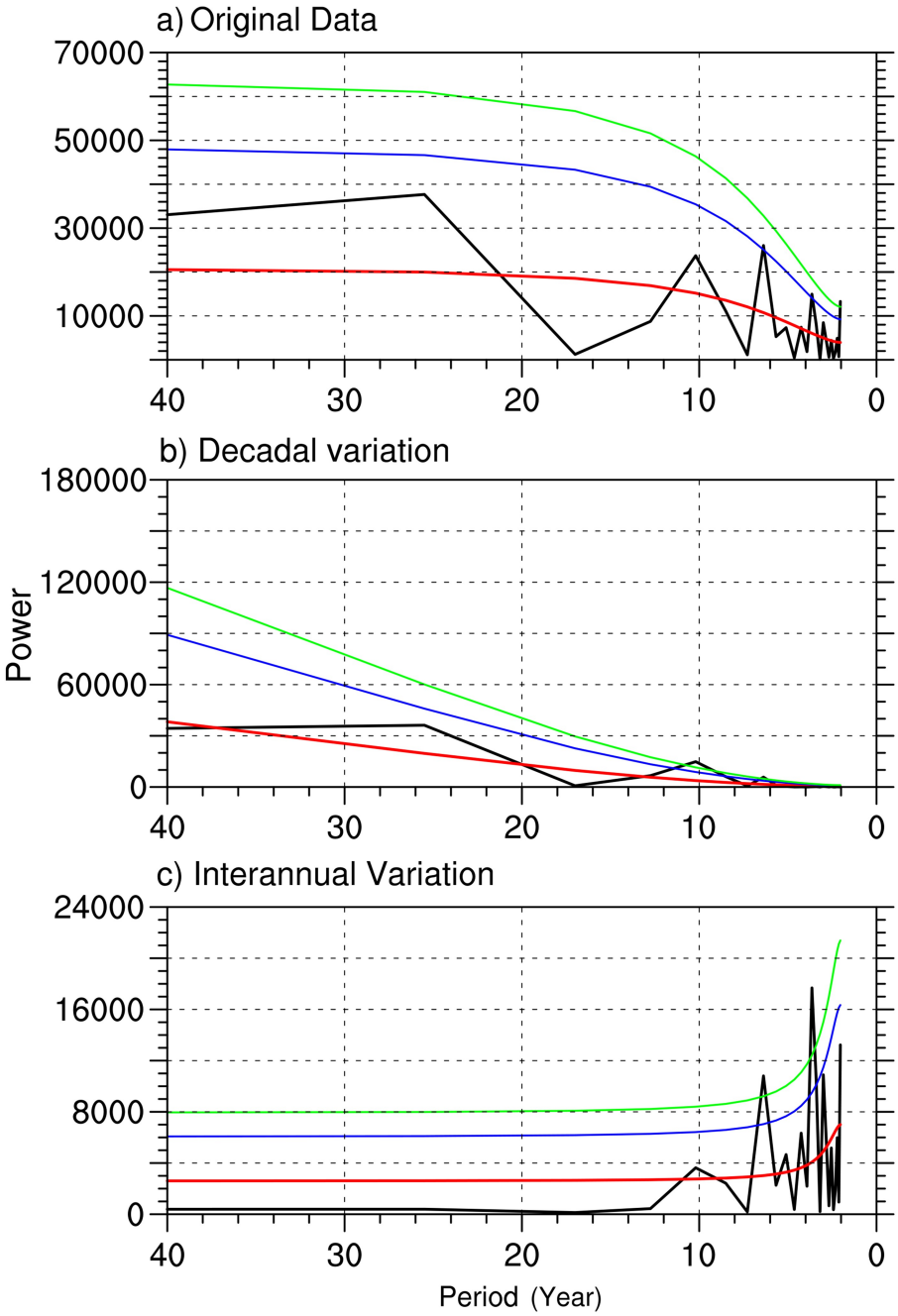

Fig. S1. The power spectrum of global total TSD (a), the decadal component of global total TSD (b), and the interannual component of global total TSD (c). The red curve indicates the red noise spectrum; the blue curve indicates the 90% confidence bound, and the green curve indicates the 95% confidence bound.

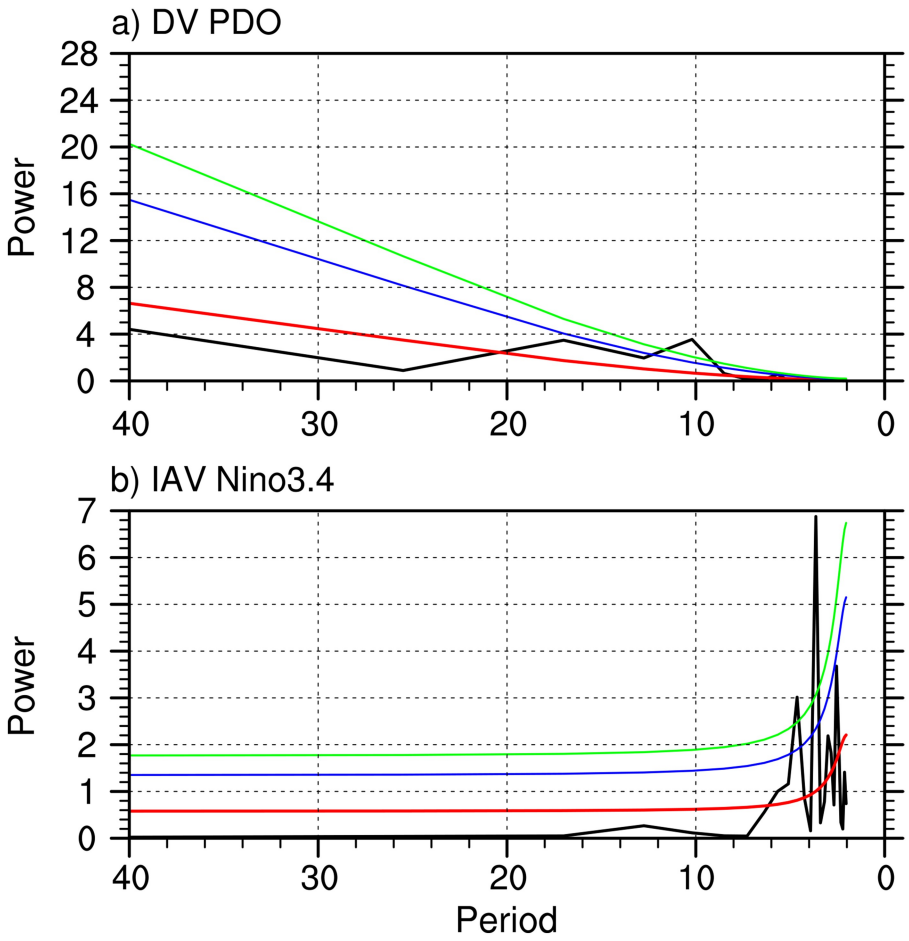

Fig. S2. Same as Fig. S1, but for (a) decadal variation of PDO and (b) interannual variation of Niño-3.4 index.

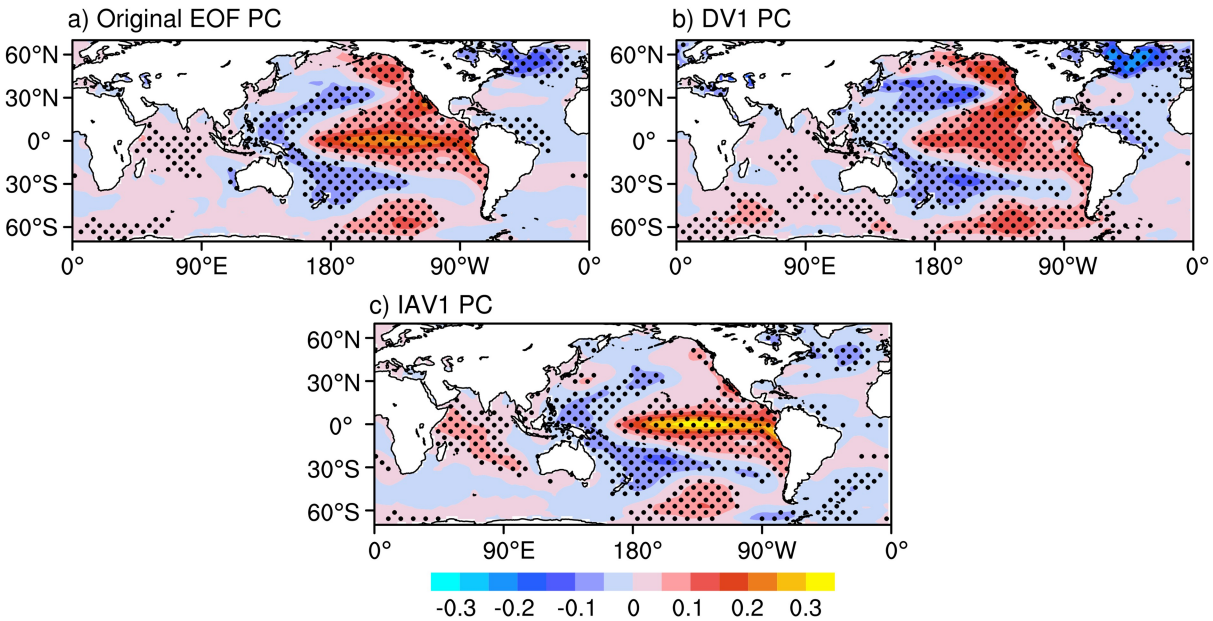

Fig. S3. Spatial distributions of regressed SST (K) against PCs of first EOF mode of (a) PC of original EOF mode, (b) DV1 PC, and (c) IAV1 PC. Dots indicate that the correlation coefficients are statistically significant at the 95% confidence level.

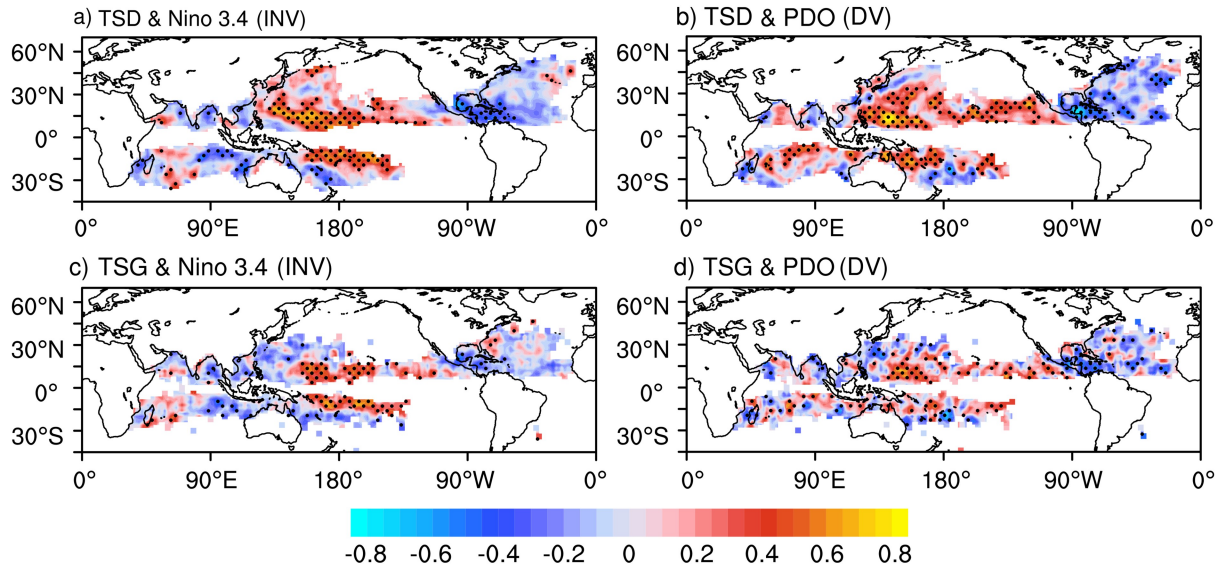

Fig. S4. The top two panels show the correlation map of global TSD and Niño-3.4 index in the interannual timescale (a), and global TSD and PDO in the decadal timescale (b). The bottom two panels show the correlation map of global TS genesis and Niño-3.4 index in the interannual timescale (c), and global TS genesis and PDO in the decadal timescale (d). Dots indicate that the correlation coefficients are statistically significant at the 95% confidence level.

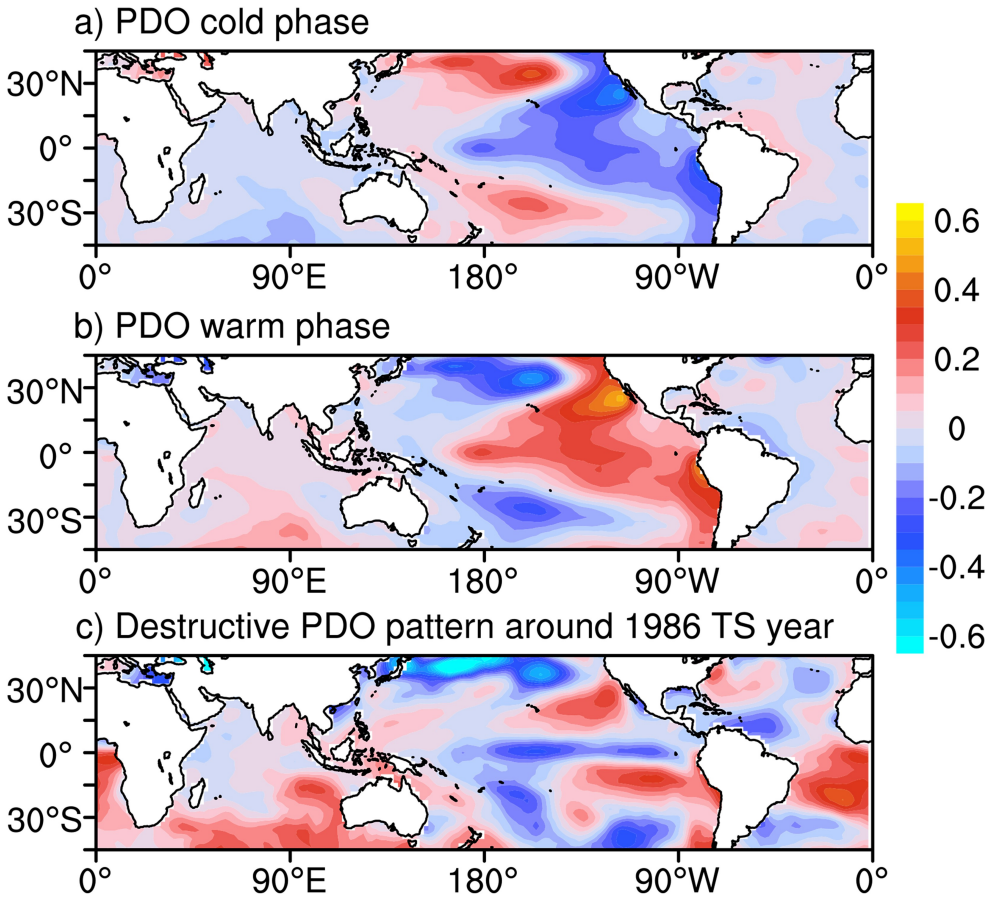

Fig. S5. The spatial distribution of SST anomalies (K) for (a) PDO warm phase, (b) PDO cold phase, and (c) destructive PDO pattern. The PDO warm phase includes the TS year from 1978 to 1997 and from 2014 to 2018, and the PDO cold phase includes the TS year from 1965 to 1977 and from 1998 to 2013. The destructive PDO pattern shown here includes the TS year from 1983 to 1989.